35th Symposium on Naval Hydrodynamics
Nantes, France, 8 – 12 July, 2024

Simulating forced drift and yaw motions of planing hulls using a numerical 2D+t method

P. Marleaux[1], H. Simonis[2], and M. Abdel-Maksoud[1]
([1]Institute for Fluid Dynamics and Ship Theory, Hamburg University of Technology, Germany, [2]Lürssen Shipyard, Germany)

ABSTRACT

A 2D+t method in combination with a numerical potential flow solver is used to simulate steady drift and yaw motions of a planing hull. A special technique is applied to model the effect of spray reattaching to the side wall and its influence on the hull forces at different forward speeds, trim angles, drift angles and heel angles is investigated. The resulting force and moment components with and without the reattachment model are compared to published experimental data. The agreement of side forces, roll and yaw moments is considerably enhanced by the reattachment model in certain conditions and generally favourable. There are some deviations in the predicted vertical lift force at high drift angles which are assumed to be caused by a low-pressure region around the keel in the potential flow solution.

INTRODUCTION

There is growing interest in efficient and accurate methods for the prediction of hydrodynamic forces on planing hulls during manoeuvring. Predictions of the hull forces as a function of the motion state can be used to assess dynamic stability which can be major safety risk at high speed. Another application is fast- or real-time motion simulation which could be used to gain information about the manoeuvring behaviour of a planing craft in certain situations or virtual training of crews for special manoeuvres. The major challenge is that forces on planing hulls are largely dominated by hydrodynamic lift which tends to be very sensitive to any change of the craft's forward speed, trim, heel or heave. Thus, hydrodynamic forces on a manoeuvring planing hull generally exhibit non-linear dependence on all six degrees of freedom (DOF). As a consequence, the number of possibly relevant motion states is increased drastically compared to the well established 3- or 4-DOF manoeuvring models which are typically used in the context of displacement hull ships. At the same time, the flow around a planing hull is characterised by strong free surface non-linearities which in turn makes their modelling particular challenging.

The classic approach to obtain a set of coefficients which express the hydrodynamic forces as a function of motion velocity and/or acceleration is conducting experiments in model scale. An extensive series of oblique towing and rotating arm tests was carried out by Brown and Klosinski (1994) who investigated different planing hull forms at various forward speeds, trim and heel angles. The results were i.a. used by Lewandowski (1997) to study transverse dynamic stability with a coupled yaw-sway-roll mathematical model. The author also reported on side wetting effects which may take place when spray attaches to the side wall of the hull and thereby increase the roll restoring moment. Toxopeus et al. (1997) and Plante et al. (1998) introduced a linearised 6-DOF manoeuvring model with coefficients obtained from planar motion mechanism (PMM) model testing and empirical formulas. Oblique towing and PMM tests by Katayama et al. (2005) in which the model was either free to heave and trim or free to heave, trim and roll confirmed the importance of those DOFs during sway and yaw motions. Based on their findings, they developed a 3-DOF simulation method in which heel, trim, heave and corresponding manoeuvring coefficients are interpolated from model test results (Katayama et al., 2006). Following this idea, so called 4+2DOF models have been presented which aim to reduce the amount of test runs that would be needed for a 6-DOF model by predicting trim and heave separately and treat them as quasi-static parameters when solving the equations of motion for the four remaining DOFs. For a recent example, see Sadati and Zeraatgar (2023).

While being considered the most reliable method, model testing is also the most elaborate one. An alternative is virtual model testing using Computational Fluid Dynamics. A recent example is given by Cura Hochbaum et al. (2022) who employed a Finite Volume Method (FVM) to compute a set of coefficients for a non-linear 3+3-DOF manoeuvring model of a planing hull. While an adequately set up FVM which solves

Reynolds Averaged Navier Stokes Equations (RANSE) in three dimensions can be expected to capture all important effects, it requires a considerable amount of computational resources to obtain a full set of coefficients.

Another group of approaches is focussed on 2D+t methods which rely on slender body assumptions. Within 2D+t theory the flow problem of a steadily moving hull is approximated by a two-dimensional (2D) unsteady flow problem within an earth fixed cross plane which the hull is passing. An early example for the use of this approach for the prediction of side forces is given by Chapman (1976) who investigated drift motions of a surface piercing flat plate. Regarding hydrodynamic forces on manoeuvring planing hulls, past 2D+t approaches mainly rely on analytical or semi-analytical flow solutions for asymmetric and oblique water entry of wedges. For instance, Xu et al. (1998) presented a flow model for asymmetric water impact of 2D wedges based on the approach by Vorus (1996) and discussed possible applications to heeled prismatic planing hulls. A similar model was developed by Judge et al. (2004) for obliquely impacting wedges which was used by Morabito (2015) to study steady drift motions of prismatic planing hulls. The agreement with experimental results was generally favourable, however the method's application range was found to be limited to high forward speed due to the zero gravity assumptions and disregarding side wetting effects. Algarín and Tascon (2011) proposed an analytical flow model for asymmetric wedge impact based on an extension of Wagner's theory (Wagner, 1932) and applied it to heeled planing hulls. The idea was extended to a model for oblique and asymmetric wedge impact to study drifting planing hulls with heel by Dashtimanesh et al. (2019). Comparisons with experiments by Brown and Klosinski (1994) showed good agreement for side forces in certain cases but also revealed discrepancies of the flow model in cases with a small trim angle and corresponding high wetted length. Nonetheless, reasonable results can be achieved when coupling the method to a 6-DOF motion solver (Tavakoli and Dashtimanesh, 2019). A similar flow model was developed by Algarín and Bula (2021) and successfully applied to solve 6-DOF manoeuvring motions. Sadati and Zeraatgar (2023) implemented a 2D+t method to calculate the roll dependent coefficients for a 4+2 DOF manoeuvring model while the other dependencies were obtained from model tests.

Recent publications show that 2D+t methods with analytical flow solutions can yield good results while being drastically less time-consuming than 3D FVM simulations or model tests. At the same time there are considerable limitations to the theoretical flow models which may compromise their accuracy in certain situations. In particular, the effect of spray reattaching to the side wall is not covered by current models which may be one reason for the observed discrepancies. A possible alternative could be a 2D+t method in conjunction with a 2D Boundary Element Method (BEM) to solve the non-linear potential flow problem numerically. In the context of planing hull hydrodynamics, such a method was proposed by Battistin and Iafrati (2003) for steady ahead forward motion and has also been applied to study symmetric motions in the vertical plane like response to head waves (Sun and Faltinsen, 2011a) or porpoising inception (Sun and Faltinsen, 2011b). Simonis et al. (2021) used the method to study yaw stability of a semi-displacement hull and obtained promising agreement for side force distributions with 3D FVM based RANSE solutions at small drift angles.

For the present study the same method has been further developed to solve the problem of steadily drifting and yawing planing hulls. The oblique towing and rotating arm experiments by Brown and Klosinski (1994) are used as a reference to assess the prediction accuracy of forces and moments. A technique for flow reattachment, which has previously been used for seakeeping analyses of semi-displacement hulls (Simonis et al., 2020), is adopted to model the effects of side wetting and investigate its influence on the results for different forward speed, drift, trim and heel conditions.

The paper is structured as follows: First, the 2D+t approach for drifting and yawing planing hulls in combination with the numerical flow solver is described. Then, the experimental conditions and corresponding simulation setups used for the study are specified. A verification of the potential flow solution obtained with the solver is shown using similarity solutions for asymmetric and oblique wedge entries from literature. Subsequently, the simulation results for straight course drifting as well as combined drift and yaw motions with and without modelling side wetting are presented and the agreement with experimental results and other 2D+t solutions are discussed.

APPROACH

Coordinate systems and kinematics

The study is concerned with a steadily moving planing hull which is forced to drift on a straight or circular course. Figures 1, 2 and 3 give an overview on coordinate systems and kinematic quantities. The usual Euler angles ψ, θ, φ are used to describe rotations of the hull. The turn rate r is the time derivative of the yaw angle ψ. The trim angle θ and the heel angle φ are not time dependent in the context of this study. An earth fixed coordinate system with axes x, y, z is used to track the hull's position and heading. The x and y axes are

located on the calm water level with the z-axis pointing downward.

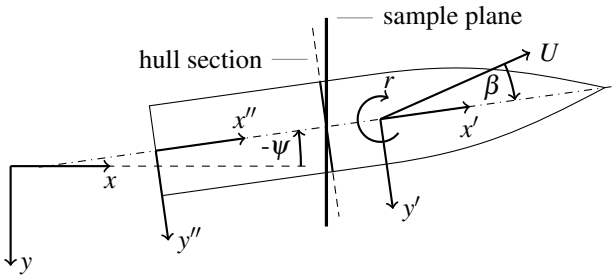

Figure 1: Coordinate systems and kinematic quantities viewed from top.

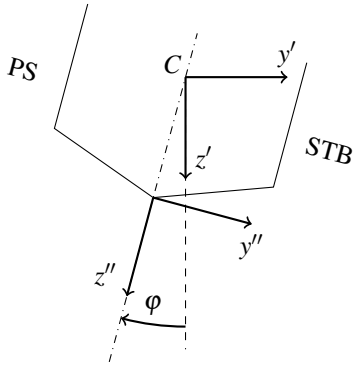

Figure 2: Coordinate systems on the hull viewed from stern.

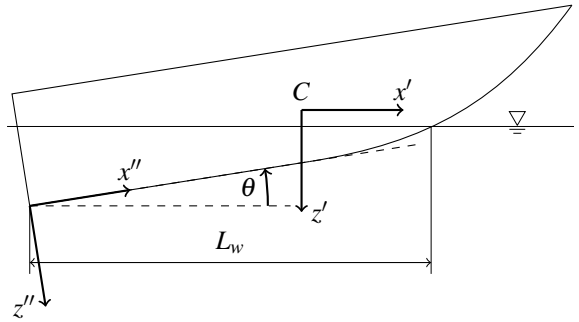

Figure 3: Coordinate systems on the hull viewed from starboard.

A semi-body-fixed system with axes x',y',z' is placed on the hull's centre of rotation C. The system follows the boat's yaw rotation but is not affected by heel or trim. The angle between the velocity vector and the x'-axis defines the drift angle β. The body-fixed system with axes x'',y'',z'' has its origin at the intersection of keel and transom stern and is affected by heel and trim. The velocity vector of a point $\boldsymbol{x_b'}$ on the hull can be described in the semi-ship-fixed system axes as:

$$\boldsymbol{v_B'} = \begin{pmatrix} U\cos\beta - r y_b' \\ -U\sin\beta + r x_b' \\ 0 \end{pmatrix}. \tag{1}$$

Transforming the velocity vector into the earth fixed system yields:

$$\boldsymbol{v_B} = \begin{pmatrix} (U\cos\beta - r y_b')\cos\psi - (-U\sin\beta + r x_b')\sin\psi \\ (U\cos\beta - r y_b')\sin\psi + (-U\sin\beta + r x_b')\cos\psi \\ 0 \end{pmatrix}. \tag{2}$$

An additional 2D coordinate system with axes ζ,η is used to describe the fluid flow within the sample plane (see Figure 4).

2D+t approach for yawing and drifting hull

The flow around the hull is approximated using 2D+t theory. As the hull moves on its given course it passes an earth fixed sample plane (see Figure 1) which, in the context of this study, is oriented parallel to the global y-z plane. The two-dimensional flow which is caused by the hull moving through that plane is calculated using a numerical flow solver.

When the hull is moving on a straight course ($r = 0$ and β between 0° and 15°) it will, in the context of this study, be oriented such that its centre plane is perpendicular to the sample plane ($\psi = 0$). This is not possible when the hull is also turning. In this case, the hull will initially be rotated by an angle ψ_0 such that the yaw angle will be close to zero when the stern passes the plane. This prevents the stern section from being cut off when it passes the sample plane at an angle. The value is calculated by multiplying the yaw rate r with the approximate time it takes for the ship to move through the sample plane:

$$\psi_0 = -r\frac{L_w}{U\cos\beta} \tag{3}$$

with L_w being the wetted length of the keel in the semi-ship-fixed coordinate system, which is also the initial distance of the stern section to the plane. Note that the drift angle β is kept constant during each simulation, no matter if the hull is moving on a straight or circular course.

The hull motion is calculated using the prescribed velocity information (U, β, r) with an explicit Euler time integration scheme. At each time step, the shape of the intersection S between sample plane and hull is passed to the flow solver along with the normal velocity

component of the hull surface $\boldsymbol{v_b} \cdot \boldsymbol{n}$ with $\boldsymbol{n}$ being the unit normal vector on the hull surface, directed out of the fluid domain and expressed in the global coordinate system. In case there is a yaw angle, the resulting pressure p will be projected to a hull section S' which is perpendicular to the centre plane (see sample plane and corresponding hull section in Figure 1) before integrating the sectional forces and moments:

$$\boldsymbol{f} = \int_{S'} p\boldsymbol{n}\sqrt{1-n_{x'}^2}ds' \tag{4}$$

$$\boldsymbol{m} = \int_{S'} p\boldsymbol{n} \times \boldsymbol{x_b'}\sqrt{1-n_{x'}^2}ds' \tag{5}$$

with s' denoting a local coordinate along the curve. The factor $\sqrt{1-n_{x'}^2}$ contains the normal component of the hull surface in x'-direction. It accounts for the obliqueness of the surface due to curvature and trim and is added to allow for a later integration of $\boldsymbol{f}$ and $\boldsymbol{m}$ along the x'-axis.

2D+t theory delivers an approximation of the three dimensional flow by taking the temporal development of the vertical and transverse flow into account. This is generally a good approximation for fast and slender bodies, where these flow components are the most dominant. However, it fails in situations where significant longitudinal flow components are induced by the body (see e.g. Iafrati and Broglia, 2010). In the case of planing hulls, the most error prone region is typically the transom stern where a sudden drop of hull pressure will be predicted instead of physically reasonable gradual decrease to atmospheric pressure. In order to account for the over-prediction of hull pressure in the stern region, a correction model developed by Soproni (2016) is applied. The model was inspired by Garme (2005) who proposed to represent the gradual reduction of the sectional hull forces with a hyperbolic tangent function. In the present model a reduction function of the following form is used:

$$f_c(l) = \begin{cases} b_1 l^{\frac{1}{2}} + b_2 l^{\frac{1}{3}} + b_1 l^{\frac{1}{4}}, & \text{if} \quad 0 \leq l \leq l_c \\ 1 & \text{if} \quad l_c < l \leq L_w \end{cases} \tag{6}$$

with L_w representing the wetted length and $l = (x' - x_T')/L_w$ the relative distance from the transom stern. The polynomial coefficients b_1 and b_2 as well the correction length l_c have been fitted by evaluating the differences in hydrodynamic lift between 2D+t BEM and 3D Finite Volume solutions for prismatic planing hulls at various deadrise angles ($15^\circ - 30^\circ$), beam based Froude numbers ($1.33 - 4$), trim ($2^\circ - 8^\circ$) and wetted length to beam rations ($3.6 - 6.6$). It has been found by Soproni (2016) that the average values $b1 = -7.278$, $b2 = 15.460$ and $l_c = 0.4$ lead to a reasonable reduction function for the whole parameter range investigated. The same values are adopted for the present study, assuming that the pressure reduction remains approximately the same at asymmetric conditions.

After the hull has completely passed the plane, the forces $\boldsymbol{F}$ and moments $\boldsymbol{M}$ are obtained by integrating the sectional values $\boldsymbol{f}$ and $\boldsymbol{m}$ over the wetted length using:

$$\boldsymbol{F} = \int_{L_w} f_c \boldsymbol{f} dx', \tag{7}$$

$$\boldsymbol{M} = \int_{L_w} f_c \boldsymbol{m} dx', \tag{8}$$

The output for $\boldsymbol{F}$ and $\boldsymbol{M}$ is generally in global coordinates but is transformed to either ship-fixed or semi-ship-fixed axes in the context of this study.

As viscosity is neglected by the flow solver, calculated resistance forces are usually under-predicted. The well known ITTC'57 correlation is used to approximate the friction forces in x'-direction:

$$F_f = \frac{0.075}{(\log_{10}(R_n) - 2)} \cdot \frac{1}{2}\rho U^2 A_w \tag{9}$$

with the Reynolds number $R_n = UL_w/\nu$ and A_w being the wetted surface area, which is obtained from integration of the sectional curve length analogous to (7) and (8).

Numerical flow solver

The unsteady flow within the sample plane is solved numerically using a Boundary Element Method (BEM) and a Mixed-Eulerian-Lagrangian (MEL) scheme to track the free surface in a non-linear fashion. The present implementation is mainly inspired by the method descriptions given by Greco (2001) and Sun (2007) and has been applied to various problems in the past (e.g Haase, 2015; Simonis et al., 2020; Marleaux et al., 2021). For the purpose of this paper only the most important characteristics and relevant features are outlined.

The general assumptions are that the flow is incompressible and irrotational which implies that viscosity is neglected and the flow velocity can be expressed as the gradient of a potential ϕ. The governing equations are the Laplace equation

$$\frac{\partial^2 \phi}{\partial \eta^2} + \frac{\partial^2 \phi}{\partial \zeta^2} = 0 \tag{10}$$

and the Bernoulli equation

$$p - p_0 = -\rho\left(\frac{\partial \phi}{\partial t} + \frac{1}{2}\left(\frac{\partial \phi}{\partial \eta}\right)^2 + \frac{1}{2}\left(\frac{\partial \phi}{\partial \zeta}\right)^2 + g\zeta\right) \tag{11}$$

which can be derived from the conservation of mass and momentum. In the above equations η and ζ denote local coordinates in the sample plane with ζ pointing upwards, t is the time, ρ the fluid density, g the gravitational acceleration, p the pressure inside the fluid and p_0 the

atmospheric pressure. A boundary value problem is formulated with following conditions:

$$\frac{D\eta_{fs}}{Dt} = \frac{\partial\phi}{\partial\eta} \tag{12}$$

$$\frac{D\zeta_{fs}}{Dt} = \frac{\partial\phi}{\partial\zeta} \tag{13}$$

$$\frac{D\phi}{Dt} = \frac{1}{2}\left(\frac{\partial\phi}{\partial\eta}\right)^2 + \frac{1}{2}\left(\frac{\partial\phi}{\partial\zeta}\right)^2 - g\zeta_{fs} \tag{14}$$

on the free surface,

$$\frac{\partial\phi}{\partial n_{2D}} = \boldsymbol{v_B}\cdot\boldsymbol{n} \tag{15}$$

on the body surface and

$$\frac{\partial\phi}{\partial n_{2D}} = 0 \tag{16}$$

on the outer boundaries. The kinematic boundary conditions (12) and (13) state that a point on the free surface boundary with coordinates (η_{fs}, ζ_{fs}) moves with the fluid velocity ($\partial\phi/\partial\eta$, $\partial\phi/\partial\zeta$) i.e. it behaves like a fluid particle. The dynamic boundary condition (14) can be derived from (11) by assuming $p = p_0$ on the free surface and making use of the definition of the substantial derivative

$$\frac{D\phi}{Dt} = \frac{\partial\phi}{\partial t} + \left(\frac{\partial\phi}{\partial\zeta}\right)^2 + \left(\frac{\partial\phi}{\partial\eta}\right)^2 \tag{17}$$

which describes the total temporal change of the potential for a fluid particle. The motion velocity of the body surface $\boldsymbol{v_B}$ is found using equation 2. The expression $\partial\phi/\partial n_{2D}$ means the derivative with respect to the normal direction of the 2D boundary while $\boldsymbol{n}$ is the three dimensional normal vector on the hull surface.

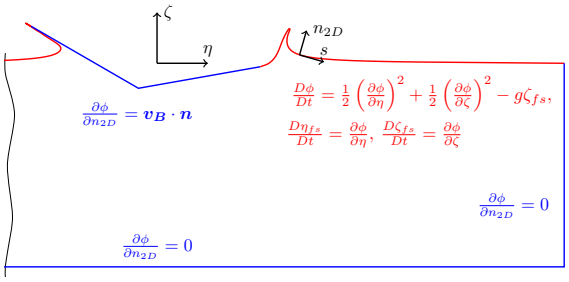

Figure 4: Sketch of boundary value problem to be solved in sample plane.

In order to solve the problem, the boundary is divided into straight line elements. Over each element a linear distribution of the boundary values ϕ and $\partial\phi/\partial n_{2D}$ is assumed. An equation system is formulated based on a general solution of the Laplace equation (10). Boundary conditions are applied by prescribing either ϕ or $\partial\phi/\partial n_{2D}$ on the nodes between elements and the missing values are found by solving the equations system. The pressure on the hull is evaluated using (11) with the time derivative of the potential $\partial\phi/\partial t$ being computed using a backward finite difference scheme.

The free surface boundary conditions are incorporated using a MEL approach. Starting with an initial solution for the free surface shape and potential, the flow velocities $\partial\phi/\partial\eta$ and $\partial\phi/\partial\zeta$ are computed using polynomial interpolation. Subsequently, the right hand sides of (12), (13) and (14) can be evaluated and the resulting time derivatives integrated using a 2nd order explicit time stepping scheme. By treating the free surface nodes like Lagrangian particles, a new free surface boundary and corresponding potential values are obtained which serve as input for solving the boundary value problem in the next time step. The free surface is frequently re-meshed to avoid instabilities and ensure an even distribution of nodes.

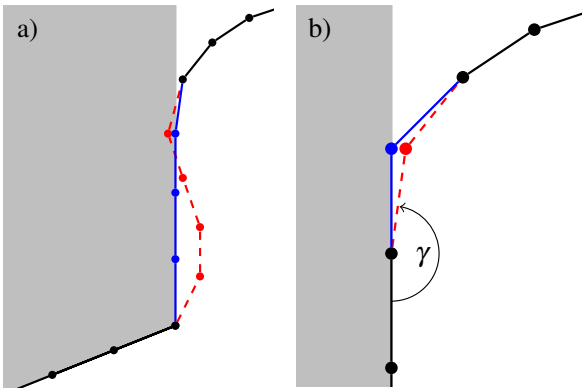

Figure 5: Sketch of reattachment technique due to intersection of free surface with hull (a) and due to formation of jet flow (b).

Various techniques are applied to account for special features of high-speed hull flow and keep the simulation stable. These include shortening of jet flow, flow separation from the chine and cutting off spray after separation (see Haase et al., 2015). Another feature, which may become relevant if the hull boundary moves obliquely, is reattachment of the separated spray to the side wall. The principle of the technique is sketched in Fig 5a. If a free surface node moves into the inner part of the hull, it will be shifted onto the hull wall and defined as the new intersection point between hull and free surface. As a consequence, the free surface nodes between the new and the previous intersection will be deleted and new nodes will be inserted on the hull surface instead. Typically a new jet flow moving up the hull

will develop in subsequent time steps which is difficult to capture numerically if the angle γ between the adjacent hull element and free surface element is too large. To overcome this issue, the free surface node next to the current intersection will be projected to the hull surface and treated as the new intersection (see Figure 5b). This will be repeated every time-step until a threshold $\gamma < \gamma_0$ is reached which allows a stable continuation of the simulation.

The model is considered a rather coarse approximation of the physical processes happening during reattachment. For instance, the air entrapped between hull and free surface is ignored and fluid pressure on the side wall is applied instantly. Nevertheless, it is believed that the overall effect is captured accurately enough to justify a continuation of the simulation beyond reattachment. The relevance of the model in the context of simulations with drifting and yawing planing hulls will be further discussed in the results section.

SIMULATION SETUP

Simulations were set up to match the experimental conditions reported by Brown and Klosinski (1994) for oblique towing as well as rotating arm tests with a planing hull model. As can be seen in the lines plan (Figure 6), the model hull is prismatic aft of the centre section (station 5). The deadrise angle of the prismatic part is 20°. The centre section is also the longitudinal position of the rotation centre C. The rudder shown in the picture was not mounted in the experiments which are used for this study. The hull geometry has been digitised from the lines plan and transferred into a 3D surface model to serve as input for the method's geometry interface. Further particulars of the model hull are summarized in Table 1.

In the experiments the model was free to heave while the other degrees of freedom were suppressed. Thus, two force and three moment components were measured in addition to the heave displacement. The reported heave displacements were used as an input for the simulations. Parameter variations included the drift angle β, the rotation radius R, trim angle θ, heel angle φ and the beam based Froude number $F_{nB} = U/\sqrt{gB}$. Table 2 shows the parameter range adopted for the straight course drift simulations and Table 3 the respective values for the simulation of rotating arm tests. The yaw rate r in the rotating arm tests can be calculated from the velocity and rotation radius which yields $r = 26.4°/s$ for $F_{nB} = 3$ and $r = 35.1°/s$ for $F_{nB} = 4$. The actual velocities used in the simulations were taken from the reported measurements. Uncertainties of setup and measurements were not reported by Brown and Klosinski (1994). Some estimates for a subset of the oblique towing tests have been made by Morabito (2015) based on their own experience with the models and apparatus. Reported uncertainty estimates are $\pm 0.2°$ for roll, trim and drift angle, $\pm 0.5B$ for wetted keel length, ± 0.01m/s for carriage speed and ± 0.5N for measurements of side force.

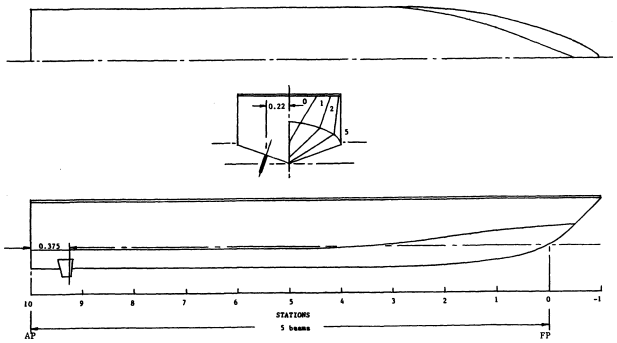

Figure 6: Lines plan of the planing hull model used in experiments by Brown and Klosinski (1994).

Table 1: Main particulars of planing hull model

Beam	B	0.2286 m
Length	L_{PP}	1.143 m
Mass	m	5.22 kg
Center of rotation	x''_C	0.5715 m
	y''_C	0 m
	z''_C	0.1054 m

Table 2: Parameter range for straight course drift simulations

Froude number	F_{nB}	3,4
Drift angle	β	$0°, 5°, 10°, 15°$
Heel angle	φ	$-10°, 0°, 10°$
Trim angle	θ	$3°, 6°$

Table 3: Parameter range for combined drift and yaw simulations

Froude number	F_{nB}	3,4
Rotation radius	R	$8.533\, L_{PP}$
Drift angle	β	$-15°$ to $15°$ in $5°$ steps
Heel angle	φ	$-10°, 0°, 10°$
Trim angle	θ	$3°, 6°$

The computational grid for the flow solver is generally divided into an inner region, with an uniform element size, and an outer region where the element size gradually increases by 10% of the respective neighbouring element. The inner region involves the hull boundary and the adjacent free surface up to a distance of one third the local beam from the hull. The outer boundaries were located $43.7B$ away from the centre. The element size was automatically adapted during simulations to account for the change of hull boundary size with time. A rather small initial element size of $\Delta s = B/2500$ was chosen for the inner region. As soon as the local hull beam within a sample plane reached a threshold of 28 elements, the flow solution was initialized. The element size first remained constant until the selected maximum of 350 elements on the hull was reached. Then, it was adjusted each time step such that the maximum of 350 hull elements is kept. Regarding the reattachment model, a threshold angle of $\gamma_0 = 90°$ was chosen.

To ensure stability of the free surface solution a maximum Courant number of

$$c = \frac{\Delta t}{\Delta s\,||\nabla\phi||} \leq 0.3 = c_{max} \tag{18}$$

was aimed for. Thus, the time step size Δt was automatically adjusted during simulations according to the flow velocity $||\nabla\phi||$ on the free surface and the respective element size. Sectional forces and corresponding boundary values were sampled every tenth time step.

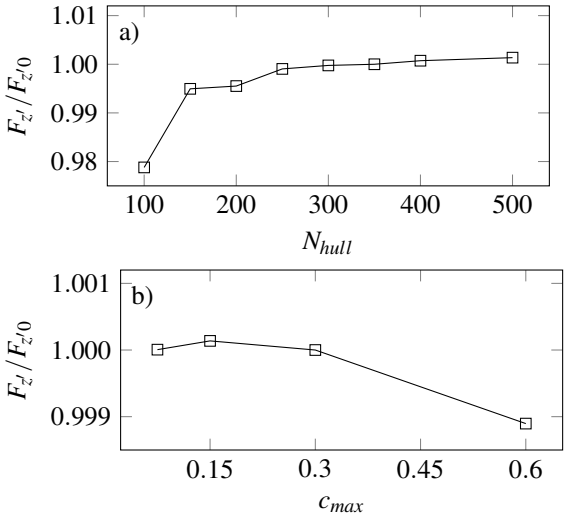

Figure 7: Dependency of vertical force on number of hull elements (a) and on maximum Courant number (b). Reference results F_{z0} are for $N_{hull} = 350$ and $c_{max} = 0.3$

The dependency of flow solution on the maximum number of hull nodes and the maximum Courant number is demonstrated for the case with $F_{nB} = 3$ $\beta = 0°$, $\theta = 3°$, $\varphi = 0°$. Figure 7 shows the change of the vertical force due to variation of those parameters is well below 1% compared higher discretisation. Note that for Figure 7b the rate with which the free surface boundary was re-meshed has been adjusted so that the graph shows only the effect of time step size on the flow solution and not the effect of more frequent re-meshing.

RESULTS

Asymmetric and oblique and wedge entry

Before looking into the 2D+t based results for planing hulls, the 2D potential flow solution obtained with the flow solver was verified by studying the impact of a 30° deadrise wedge with $-10°$ heel. Simulations were carried out with the zero-gravity assumption and stopped before flow separation from chines occurred in order to obtain a similarity solution. The pressure distribution is compared to an analytical solution for asymmetric vertical impact by Semenov and Iafrati (2006) in Figure 8. The agreement is very good except at a small region left of the wedge apex where the analytical model predicts higher pressure. Two oblique impact cases with transverse to vertical velocity ratios of $v/w = 0.5$ and $v/w = -0.5$ are considered as well and compared to numerical results by Xu et al. (2008) with good agreement.

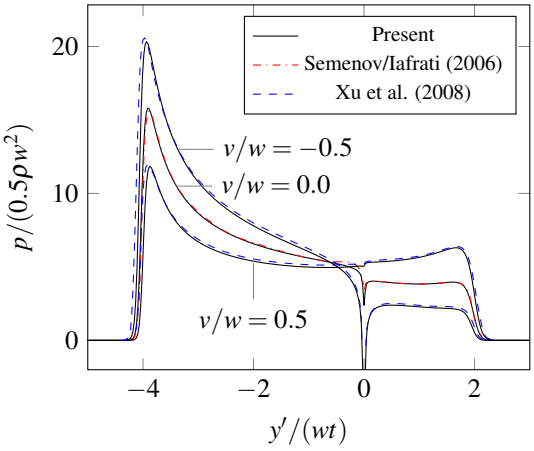

Figure 8: Comparison of calculated pressure distribution on vertically and obliquely impacting wedges with 30° deadrise and $\varphi = -10°$ heel angle with published similarity solutions.

The Figure demonstrates which effects on the hydrodynamic forces can be expected in the forward region of a drifting hull which is heeled. The heel angle causes higher pressure on the side with smaller effective

deadrise angle (i.e. negative y' in this case) which leads to a side force and corresponding moments. The effect is increased when hull drifts in this direction and reduced if it drifts in the opposite direction. There is a pressure drop around the wedge apex which appears to be more pronounced when the peak pressure difference between the two sides is higher.

Straight course drift simulations

In the following, the forces and moments obtained with the numerical 2D+t method from simulation of steady drift and yaw motions of a planing hull are presented and discussed, starting with the straight course drift simulations. Each condition specified in Tables 2 and 3 was carried out with and without using the reattachment technique, which yields a total number of 264 simulations. Thereof, 12 simulations could not be completed without modelling reattachment. Simulation of a single case took about 20-30min using one processor core. Using a workstation with 12 cores (Intel® Xeon® Gold 5118 CPU @ 2.30GHz), the whole set of computations could be completed in less than 10h. In comparison, a realistic wall clock time for simulating a single case with a 3D FVM on one processor core is about 2-3 days (Cura Hochbaum et al., 2022).

Figure 9 shows a comparison of the six force and moment components resulting from the oblique towing tests by Brown and Klosinski (1994) and the respective simulation with $F_{nB} = 3$ and $\theta = 3^\circ$ at different heel angles. Regarding the x'-component, there are large deviations of the pure potential flow results from the experimental measurements. The agreement is drastically improved when the friction force (9) is added, which emphasizes the importance of shear forces for resistance prediction of planing hull.

The side force $F_{y'}$ generally agrees very well with the experimental results at lower drift angles and tends to be somewhat under-predicted at higher drift angles. A positive heel angle generally leads to less side force and better agreement. Note that the vertical axes in the plots are scaled to the data range. With positive heel, the reattachment technique has a little influence at zero drift and is irrelevant for the other drift angles. At zero heel, results are greatly improved by the technique and its relevance increases with drift angle. At negative heel, simulations for $\beta = 10^\circ$ and $\beta = 15^\circ$ could not be completed without modelling side wetting, because the spray reached so far into the inner part of the hull that the free surface boundary intersected with the hull bottom boundary causing the simulation to abort. Agreement is quite favourable given that the conditions are rather extreme and large velocities around the keel can be expected in the potential flow solution at $\beta = 15^\circ$.

The vertical force $F_{z'}$ was not measured in the experiments. However, as the model was free to heave, the fluid force acting on the hull needs to be in balance with the gravitational force mg. Note that z' is pointing vertically downward which is why $F_{z'}$ has a negative sign in the plots. At zero heel and drift the absolute value of the force is over-estimated by about 12.6%. A reason for this could be 3D effects in the region of chine separation which are not accounted for by the current correction model. Also, uncertainties in the experimental conditions (e.g. heave measurement, adjustment of trim and model mass) could have a higher influence on the predicted vertical force and trim moment than on other components. For instance, a change of the trim angle in the straight ahead simulation of about $\pm 0.2^\circ$, which is the estimated uncertainty for the trim angle, leads to a change of about $\pm 0.06\,mg$ in the resulting vertical force and $\pm 0.1\,mgB$ in the trim moment.

Apart from the error at zero heel and drift, the predicted lift force tends to decrease when the hull is heeled to any direction and also at higher drift angles. An extreme example can be seen with $\beta = 15^\circ$ and $\varphi = -10^\circ$ which is clearly erroneous. The reason for this behaviour is most likely the negative pressure area which occurs around the keel in the potential flow solution (see Figure 8) and becomes more dominant at high drift angles (see Figure 10).

The predicted roll moment $M_{x'}$ agrees fairly well with the experimental measurement and is clearly influenced by side wetting at zero and negative heel. The dependency of the trim moment $M_{y'}$ on drift and heel seems to be reproduced well. There is a nearly constant negative offset which might be related to the over-prediction of lift at non-heeled straight ahead conditions. Regarding the yaw moment $M_{z'}$, the agreement is very good with a positive heel angle. At zero and negative heel the effect of side wetting is particularly strong. The results agree well for $\beta = 5$ and start to deviate at higher drift angles.

Figure 10 shows the pressure distribution on the hull bottom for the simulated oblique towing tests (middle column in Fig 9). Note that the correction function (6) is applied to the sectional force and not directly to the pressure which is why a reduction towards the stern is not visible here. The figure demonstrates that there is a strong pressure increase at one of the spray roots due to drift which can be seen as the main cause for side forces in the forward region. It also shows the low-pressure region around the keel, which becomes more severe with higher transverse velocities and is probably the main reason for the observed deviation of $F_{z'}$ from a constant value at high drift angles. The side force $F_{y'}$ is presumably less affected, because the pressure drop extends over both sides of the keel.

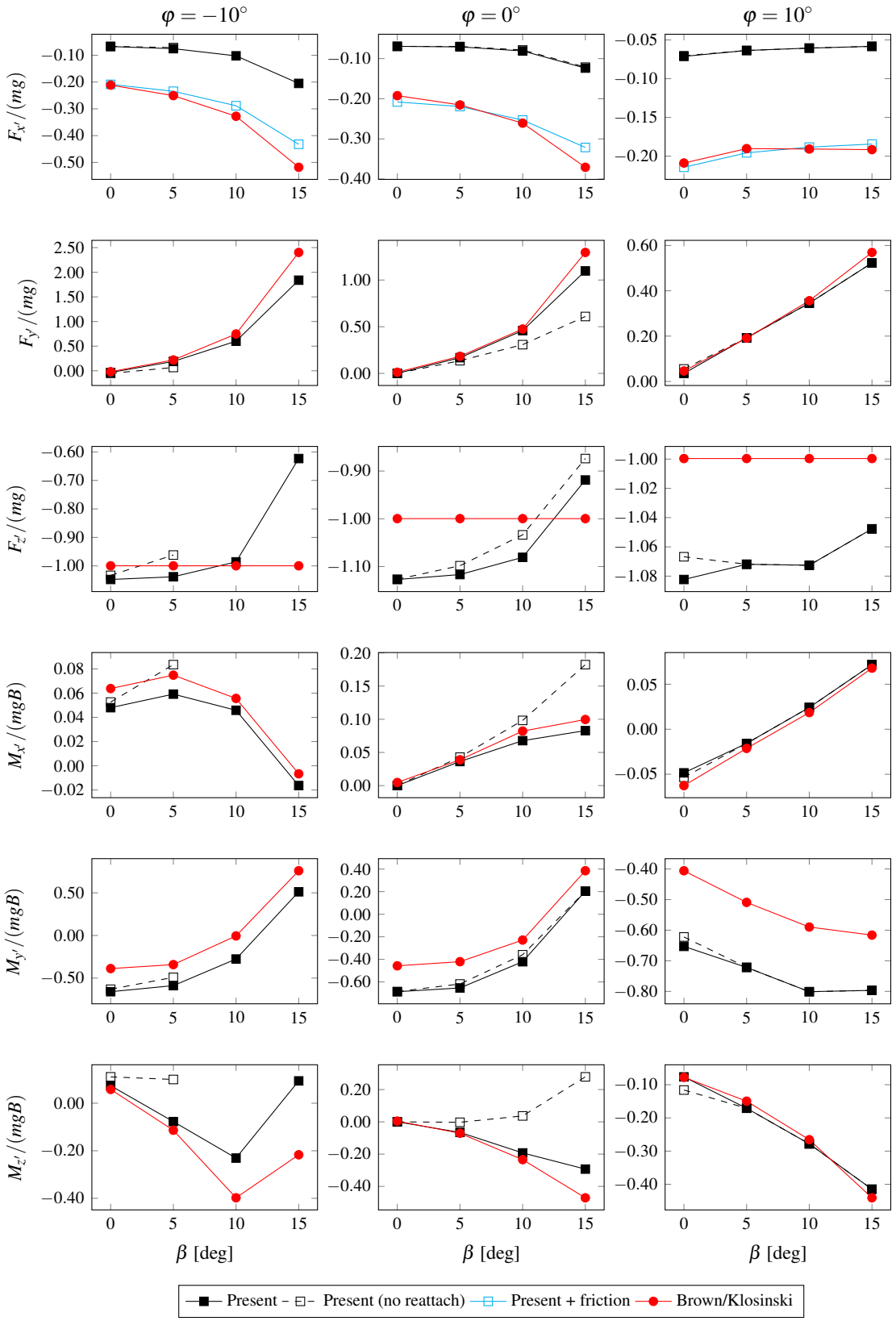

Figure 9: Calculated forces and moments for straight course drift simulations with $\theta = 3°$, $F_{nB} = 3.0$ in semi-body-fixed system compared to experimental results by Brown and Klosinski (1994).

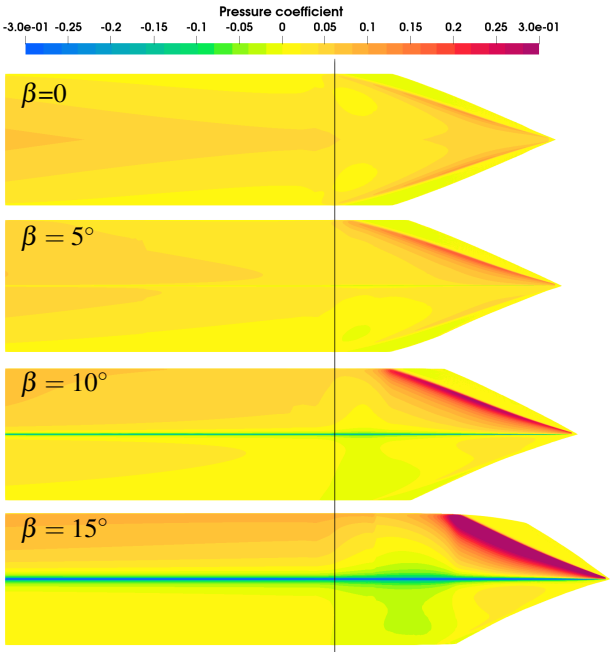

Figure 10: Pressure distributions on the hull bottom for straight course drift simulations with $F_{nB} = 3$, $\theta = 3°$ and $\varphi = 0°$. Black line indicates centre section.

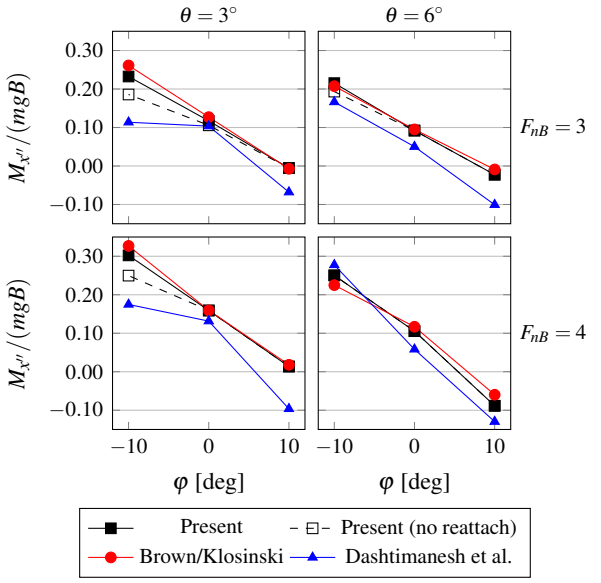

Figure 12: Moment around body fixed x''-axis versus heel angle from straight course drift simulations with $\beta = 5°$ for different trim angles and forward speeds compared to experimental results by Brown and Klosinski (1994) and 2D+t results with analytical flow solution by Dashtimanesh et al. (2019).

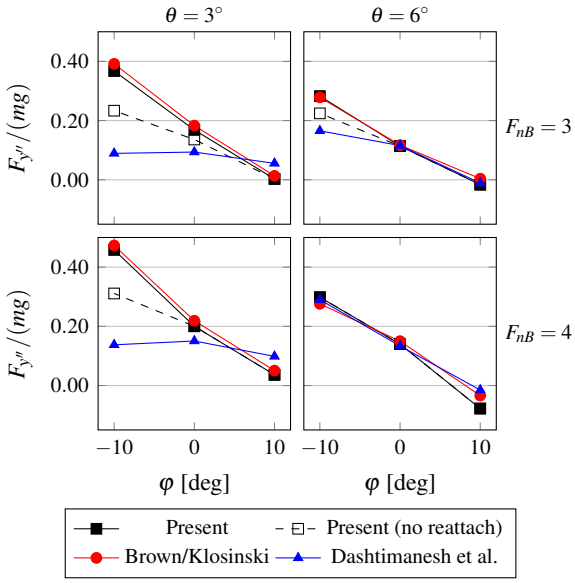

Figure 11: Force in body fixed y''-direction versus heel angle from straight course drift simulations with $\beta = 5°$ for different trim angles and forward speeds compared to experimental results by Brown and Klosinski (1994) and 2D+t results with analytical flow solution by Dashtimanesh et al. (2019).

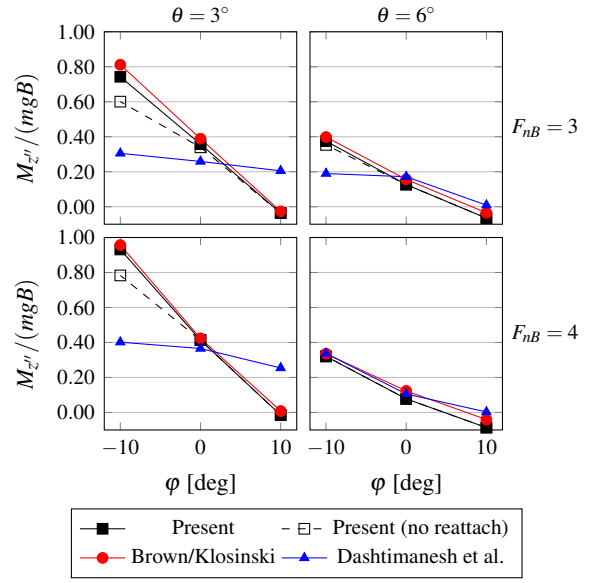

Figure 13: Moment around body fixed z''-axis from straight course drift simulations with $\beta = 5°$ for different trim angles and forward speeds compared to experimental results by Brown and Klosinski (1994) and 2D+t results with analytical flow solution by Dashtimanesh et al. (2019).

It can be expected that in reality the flow will not follow the sudden change of the body contour at the keel but separate instead. 2D RANS computations of obliquely impacting wedges (e.g. Yang and Xu, 2018) indicate that vortex separation will cause a low-pressure region to develop on the leeward side but an extreme pressure drop as predicted by potential theory is avoided. This can also be seen in the pressure distribution published by Cura Hochbaum et al. (2022) for a planing hull with high drift angles. There have been attempts to include this effect within the scope of potential flow theory by modelling a separated vortex sheet and invoking a Kutta-condition at the corner point which prevents the flow from passing directly over it (e.g. Riccardi and Iafrati, 2004 or Semenov and Wu, 2018). An possible implementation in a BEM has been proposed by Xu and Wu (2015) using discrete vortex elements which are tracked in time. Implementing such a technique in the present flow solver could be a way to improve the prediction accuracy of vertical and transverse forces at high drift angles.

The whole set of the resulting forces and moments from the straight course drift simulations can be found in Figure 20 of the Appendix. The effect of forward speed, trim angle and heel is demonstrated for a drift angle of $\beta = 5°$ in Figures 11, 12 and 13 which show the computational and experimental values for $F_{y''}$, $M_{x''}$ and $M_{z''}$ versus φ for two trim angles and Froude numbers respectively. The forces and moments are expressed with respect to the ship-fixed coordinate system to allow for a comparison with the results by Dashtimanesh et al. (2019) who studied the same cases using 2D+t theory with a model based on a modified Wagner solution.

For the lower trim angle $\theta = 3$, the numerical method matches the experiments very well while the analytical flow solution does not seem to be appropriate. Deviations also occur in cases without side wetting, which indicates that other limits of the theoretical flow model might be exceeded as well. Increasing the forward speed at $\theta = 3$ removes the side wetting effect for the zero heel condition. Force and moment values are slightly increased due to the speed increase which is reflected well by the numerical method.

Regarding $\theta = 6$, side wetting only plays a role at the lower speed with negative heel. The theoretical results and the numerical results without the reattachment technique for $F_{y''}$ and $M_{z''}$ deviate from the measurements at this condition. For the other conditions, both methods yield satisfactory agreement with the moment $M_{x''}$ being a bit better represented by the numerical results. The numerical results show some deviation for $F_{y''}$ at $F_{nB} = 4$ and $\varphi = 10$ which might be related to the error in vertical force as it influences $F_{y''}$ through the transformation to the ship-fixed system. Compared to the lower trim angle, the curves for $F_{y''}$ and $M_{x''}$ are less steep and tend to be shifted downward which is replicated satisfactorily by the present method. The reduced relevance of side wetting with increased speed and trim angle might be explained by a reduction of the wetted length which makes it less likely that spray interacts with the side wall. The change of the wetted length due to trim and forward speed is demonstrated in Table 4 for the zero heel cases at $\beta = 5°$. The values do not account for water pile up and are taken from the test report by Brown and Klosinski (1994).

Table 4: Ratio of static keel wetted length to beam reported by Brown and Klosinski (1994) for $\beta = 5°$ and $\varphi = 0°$.

	L_w/B	
	$\theta = 3°$	$\theta = 6°$
$F_{nB} = 3$	4.23	2.17
$F_{nB} = 4$	3.95	1.39

Combined drift and yaw simulations

In the following, simulation results for combined drift and yaw motion of the hull are presented and compared to the rotating arm test results. Figure 14 shows the force and moment components as function of the drift angle for $F_{nB} = 3$ and $\theta = 3°$. It can be seen that the dependence of force and moment components on the drift angle during a yaw rotation is generally replicated well by the numerical method. With a positive heel angle the agreement tends to get worse at high negative drift angles and vice versa. This is probably related to greater flow velocities across the keel at these conditions which leads to under-predicted side forces and reduced vertical force as already discussed. At zero heel, the vertical force deviates noticeably from a constant value for drift angles greater than $\pm 5°$.

As for the straight course drift simulations, the reattachment technique greatly improves the agreement with experimental data and some simulations could not even be finished without it. This applies to all the cases with negative drift angle when the heel angle was $\varphi = 10°$. The same applies to a heel angle of $\varphi = -10°$ for cases with $\beta = 10°$ and $\beta = 15°$. At zero heel, the reattachment technique improves the results for both, positive and negative drift angles. Especially the yaw moment is strongly influenced, even at the small drift angle of $\beta = 5°$. Figure 15 shows the distribution of sectional side force $f_{y'}(x')$ for this case, compared to the straight course drifting simulation. With yaw rotation side wetting happens further forward and causes a much stronger impact which is most likely a consequence of the increased transverse velocity at the aft sections. The Figure also reveals a weakness of the reattachment model,

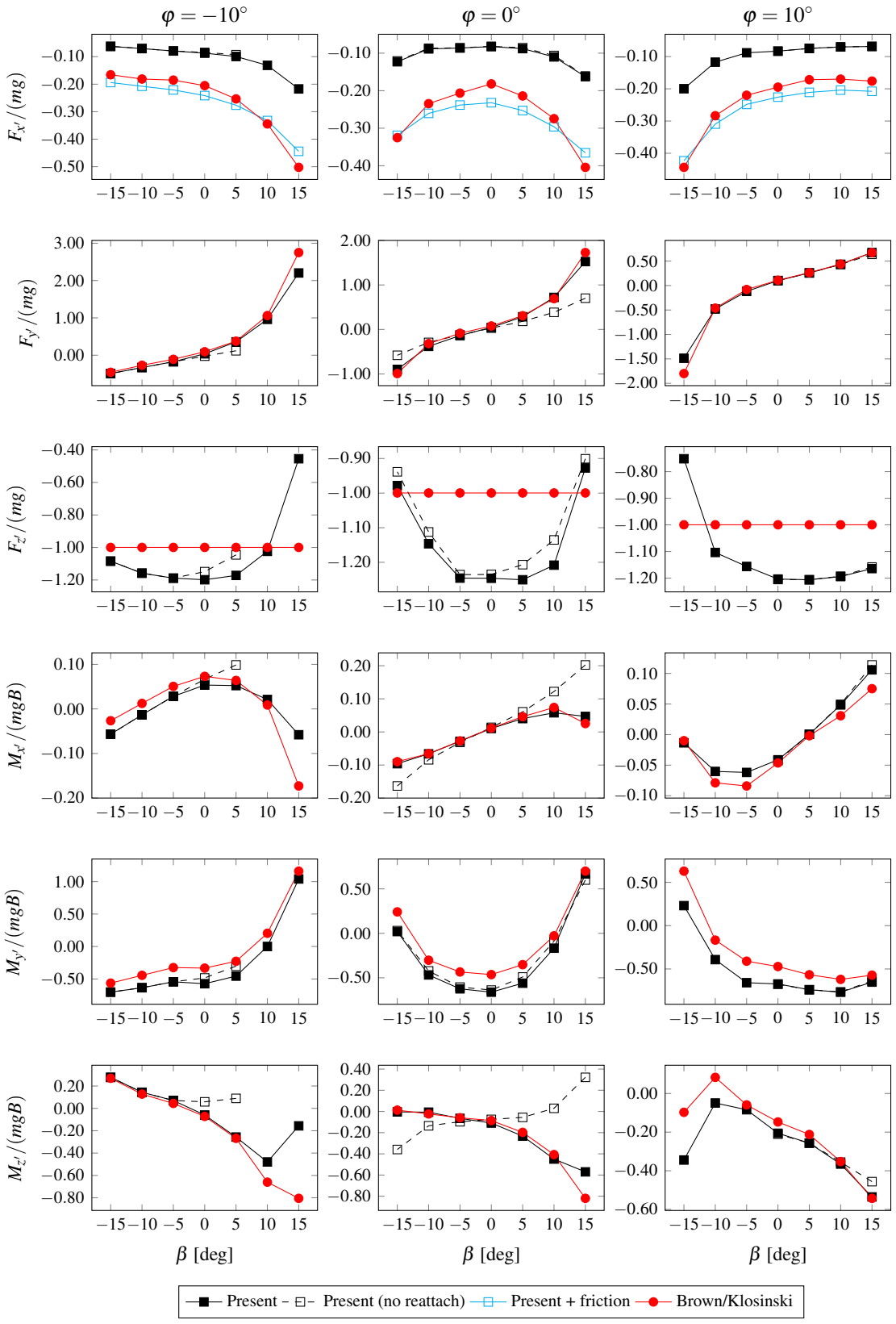

Figure 14: Calculated forces and moments for combined drift and yaw simulations with $\theta = 3°$, $F_{nB} = 3.0$ in semi-body-fixed system compared to experimental results by Brown and Klosinski (1994).

which is that the side wall is assumed to be instantly wetted as soon as an intersection between free surface boundary and hull geometry is detected. Thus, pressure is applied to the side wall from one time-step to the other which leads to a very steep increase of sectional force. Nonetheless, the error introduced by these assumptions can be considered much lower than the errors made by neglecting the side wetting. Figure 16 demonstrates the difference between free surface shapes at the aft section with and without using the reattachment technique.

Figure 17 shows the pressure distribution at the same conditions as in Figure 10 but with the addition of yaw rotation. It can be seen that an additional asymmetry is induced by the rotation, which is most pronounced at the stern. This can be explained by the large distance to the rotation centre.

The whole set of the resulting forces and moments from the combined drift and yaw simulations can be found in Figure 21 of the Appendix. The influence of trim angle and velocity on the results in comparison with the straight course drift results is demonstrated in Figures 18 and 19 which show the force $F_{y'}$ and the moments $M_{z'}$ for $\beta = 5°$ with and without yaw rotation

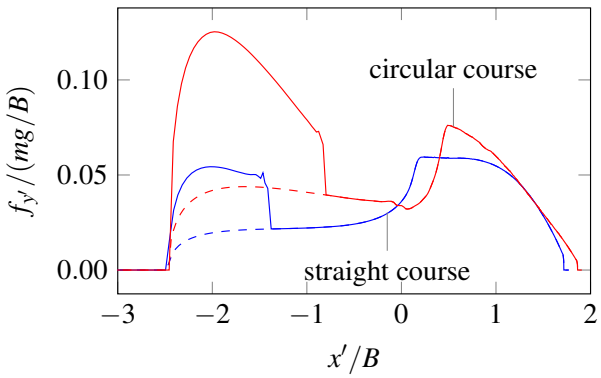

Figure 15: Distribution of side force versus length for $F_{nB} = 3$, $\beta = 5$, $\theta = 3°$ and $\varphi = 0°$ for pure drift and combined drift and yaw motions respectively. Dashed lines indicate results without the reattachment technique

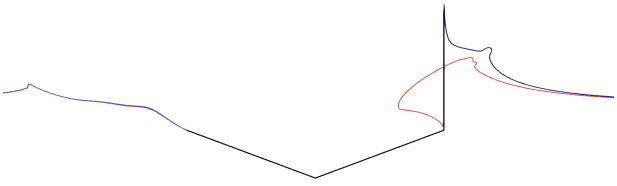

Figure 16: Free surface shapes at the stern section in simulations with (blue) and without (red) flow reattachment for combined drift and yaw simulation with $F_{nB} = 3$, $\theta = 3°$ and $\varphi = 0°$, $\beta = 5°$.

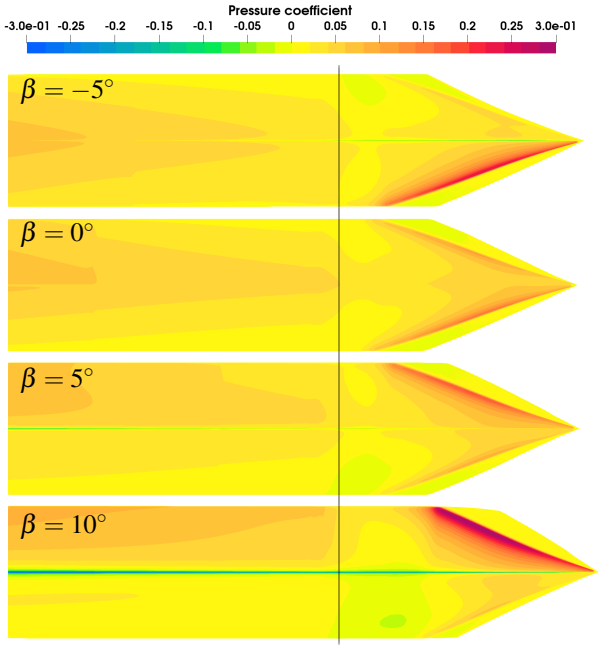

Figure 17: Pressure distributions on the hull bottom for combined drift and yaw simulations with $F_{nB} = 3$, $\theta = 3°$ and $\varphi = 0°$. Black line indicates centre section.

as a function of the roll angle for different velocities and trim angles. For most cases the simulation results show the same trends with regard to the parameter variations as the experimental data. An exception is the case with positive heel. While there is good agreement with $F_{nB} = 3$ and $\theta = 3°$, the data tend to deviate when the speed or the trim angle increases. A possible reason could be that 3D effects at the stern are not correctly accounted for in highly asymmetric conditions and with small wetted length. The correction model for pressure reduction towards stern (6) was calibrated on symmetric cases with wetted length greater than $L_w = 3.6B$. Thus, an adjustment of the function might be necessary for smaller values. In addition, it can be expected that 3D effects in the forward regions of the hull are more dominant at smaller wetted length. Comparisons of pressure distributions with 3D FVM simulations could be a way to gain more insight.

Regarding an application of the method to manoeuvring simulations, it should be noted that not all of the configurations tested in the free to heave model experiments, which were reproduced in this study, do necessarily reflect realistic situations. For instance, the typical steady state in a starboard turning manoeuvre of a planning boat is a positive drift angle and a positive heel angle (see Katayama et al., 2006). Other combinations of drift and heel angle

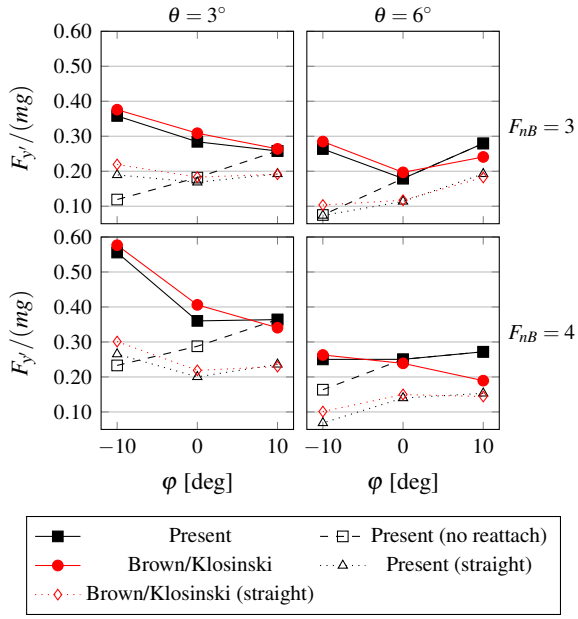

Figure 18: Side force $F_{y'}$ versus heel angle from combined drift and yaw simulations with $\beta = 5°$ for different trim angles and forward speeds as well as respective results from straight course drift simulations compared to experimental results.

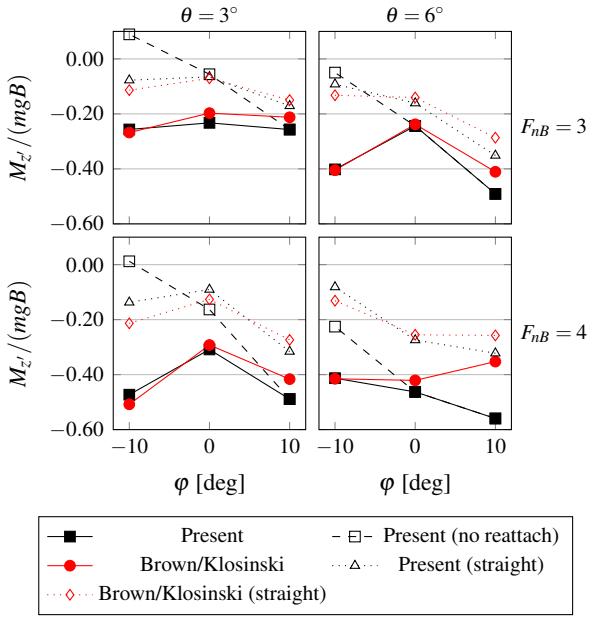

Figure 19: Yaw moment $M_{z'}$ versus heel angle from combined drift and yaw simulations with $\beta = 5°$ for different trim angles and forward speeds as well as respective results from straight course drift simulations compared to experimental results.

are thinkable as well, e.g. due to change of turning direction, unsymmetrical loading or environmental influences. However, a state with large positive drift angle and negative heel angle, which would clearly exceed the limitations of the potential flow solver (see left columns of Figures 9 and 14 at $\beta = 15°$), can be considered rather unlikely. Nonetheless, the systematic variations conducted in this study provide insights into the method's strengths and limitations under various conditions, which can serve as a basis for future developments and improvements.

CONCLUSION

In summary, the numerical 2D+t method with reattachment technique is found to be a viable tool for predicting side forces and corresponding moments on the planing hull investigated at steady drift or combined drift and yaw conditions. Depending on the roll angle, there is a tendency of under-prediction of the side forces at high drift angles, which is mitigated to a large extent by modelling the side wetting effect. The influence of side wetting is especially pronounced at smaller trim angle and lower speed, which reflects a situation with relatively high wetted length in the free to heave experiments. The effect also tends to become more relevant if an additional yaw rotation is considered. Being able to model the influence of gravity on the spray flow and include possible side wetting effects, enhances the range of applicability of the present method compared to 2D+t theory in combination with a flow model based on enhanced Wagner theory.

The tool is considered less reliable for prediction of vertical forces. While the over-prediction of lift force at straight ahead condition might be a combination of omitted 3D-effects and uncertainties in the experimental setup, there is also a tendency toward decreasing lift with drift and heel angle. This is most likely related to an over-prediction of flow velocities around the keel in the potential flow solution which leads to a narrow area of highly negative pressure at both sides of the keel.

Implementing a wake model to consider vortex shedding at the keel could be a way to enhance the current flow solver in that regard. Future works may also include direct comparison with pressure distributions obtained using 3D RANS computations to verify the reattachment technique and gain more insight on 3D effects during drift and yaw motions. This might help to clarify the reasons for the observed over-prediction of lift force as well as side forces in certain parameter combinations for the combined drift and yaw simulations.

For an future application to manoeuvring simulations there are two possible ways: Firstly, the method could be used to compute coefficients for a mathematical manoeuvring model, which would

allow calm water simulation in a very efficient way. Secondly, the simulation setup could be altered such that multiple sample sections are placed into the fluid domain and the unsteady motion of the hull is solved directly in conjunction with the flow (Simonis et al., 2021). Simulating a manoeuvre like this would be arguably more time-consuming but the setup would allow consideration of environmental influences like waves on the manoeuvring behaviour which are difficult to reflect in a coefficient based method.

ACKNOWLEDGEMENTS

This work was supported by the German Federal Ministry of Defence under the administration of the Technical Centre for Ships and Naval Weapons, Maritime Technology and Research (WTD 71). The authors sincerely thank Dr. Norbert Stuntz for the scientific support and fruitful discussions.

REFERENCES

Algarín R. and Bula, A., "A numeric study of the maneuverability of planing hulls with six degrees of freedom," Ocean Engineering, Vol. 221, 2021, p. 108514.

Algarín R. and Tascon O., "Hydrodynamic Modeling of Planing Boats with Asymmetry and Steady Conditions," Proceedings of 9th Symposium on High Speed Marine Vehicles, 25-27 May, 2011, Naples, Italy.

Battistin D. and Iafrati, A., "A Numerical Model for Hydrodynamics of Planing Surfaces," Proceedings of the 7th International Conference on Fast Sea Transportation, 2003, Ischia, Italy.

Brown, P.W. and Klosinski, W.E., "Directional Stability Tests of Two Prismatic Planing Hulls," CG-D-11-94, 1994, Davidson Laboratory, Stevens Institute of Technology, Hobooken, New Jersey, USA.

Chapman R.B., "Free-Surface Effects for Yawed Surface-Piercing Plates", Journal of Ship Research, Vol. 20, No. 3, 1976, p. 125–136.

Cura Hochbaum, A., Blum, B., and Uharek, S., "A novel 3+3 DOF method for manoeuvring prediction of planing boats," Proceedings of the 34th Symposium on Naval Hydrodynamics, June 26-July 1, 2022 Washington DC, USA.

Dashtimanesh, A., Enshaei, H., and Tavakoli, S., "Oblique-asymmetric 2D+T Model to Compute Hydrodynamic Forces and Moments in Coupled Sway, Roll and Yaw Motions of Planing Hulls," Journal of Ship Research, Vol. 63, No. 1, 2019.

Garme, K., "Improved time domain simulation of planning hulls in waves by correction of the near-transom lift," International Shipbuilding Progress, Vol 52, No. 3, 2005, pp. 201-230.

Greco, M., "A Two-dimensional Study of Green-Water Loading," PhD thesis, Norwegian University of Science and Technology, Trondheim, 2001.

Haase, H., Soproni, J.P., and Abdel-Maksoud, M., "Numerical analysis of planing boats in head waves using a 2D+t method," Ship Technology Research, Vol. 62, No. 3, 2015, pp. 131-139.

Iafrati, A. and Broglia, R., "Comparison between 2D+t potential flow models and 3D RANS for planing hull hydrodynamics" Proceedings of the 25th International Workshop on Water Waves and Floating Bodies, 9-12 May, 2010, Harbin, China.

Judge, C., Troesch. A., and Perlin, M., "Initial water impact of a wedge at vertical and oblique angles," Journal of Engineering Mathematics, Vol. 48, 2004, pp. 279-303.

Katayama, T., Kimoto, R., and Ikeda, Y., "Effects of running attitudes on maneuvering hydrodynamic forces for planing hulls," Proceedings of the 8th International Conference on Fast Sea Transportation, 27-30 June, 2005, St. Peterspurg, Russia.

Katayama, T., Iida, T., and Ikeda, Y., "Effects of Change in Running Attitude on Turning Diameter of Planing Craft," Proceedings of 2nd PAAMES and AMEC2006, 17-20 October, 2006, Jeju Island, Korea.

Lewandowski, E.M., "Transverse dynamic stability of planing craft," Marine Technology, Vol. 34, No. 2, 1997, pp. 109-118.

Marleaux, P., Simonis, H., and Abdel-Maksoud, M., "Time domain simulations of piston-like resonant flow in the gap of an oscillating twin-hull using inviscid and viscous flow solvers," Ocean Engineering, Vol. 223, 2021, p. 108672.

Morabito, M.G., "Prediction of planing hull side forces in yaw using slender body oblique impact theory," Ocean Engineering, Vol. 101, 2015, pp. 47-57.

Plante, M., Toxopeus, S., Blok, J., and Keuning A., "Hydrodynamic manoeuvring aspects of planing craft," Proceedings of the International Symposium and Workshop on Forces Acting on a Manoeuvring Vessel, September, 1998, Val de Reuil, France.

Riccardi, G. and Iafrati, A., "Water impact of an asymmetric floating wedge," Journal of Engineering Mathematics, Vol. 49, 2004, pp. 19-39.

Sadati, K. and Zeraatgar, H., "Simulation of turning maneuver using the 4+2 DOF method in planing and semi-planing modes," Ocean Engineering Vol. 287, 2023, p. 115763.

Semenov, Y.A. and Iafrati, A., "On the nonlinear water entry problem of asymmetric wedges," Journal of Fluid Mechanics, Vol. 547, 2006, pp. 231-256.

Semenov, Y.A. and Wu, G.X., "Water entry of a wedge with rolled-up vortex sheet," Journal of Fluid Mechanics, Vol. 835, 2018, pp. 512-539.

Simonis, H., Marleaux, P., and Abdel-Maksoud, M., "Numerical analysis of semi-displacement vessels in head waves," Proceedings of the 33rd Symposium on Naval Hydrodynamics, 18-23 October, 2020, Osaka, Japan.

Simonis, H., Marleaux, P., and Abdel-Maksoud, M., "Dynamic stability analysis of a ship at high forward speed in calm water," Proceedings of the 23rd Numerical Towing Tank Symposium, 11-13 October, 2021, Mühlheim an der Ruhr, Germany.

Soproni, J.P., "Bestimmung hydrodynamischer Eigenschaften von Gleitbooten mithilfe einer Randelementmethode und der 2D+t Theorie", PhD thesis, Hamburg University of Technology, Germany, 2016.

Sun, H., "A Boundary Element Method Applied to Strongly Nonlinear Wave-Body Interaction Problems", PhD thesis, Norwegian University of Science and Technology, Trondheim, 2007.

Sun, H. and Faltinsen, O.M., "Dynamic motions of planing vessel in head seas," Journal of Marine Science and Technology, Vol. 16, No. 2, 2011a, pp. 168-180.

Sun, H. and Faltinsen, O.M., "Predictions of porpoising inception for planing vessels," Journal of Marine Science and Technology, Vol. 16, No. 3, 2011b, pp. 270-282.

Tavakoli, S. and Dashtimanesh, A., "A six-DOF theoretical model for steady turning maneuver of a planing hull," Ocean Engineering, Vol. 189, 2019, p. 106328.

Toxopeus, S.L., Keuning, J.A., and Hooft, J.P., "Dynamic stability of planing ships," Proceedings of the International Symposium and Seminar on the Safety of High Speed Craft, February, 1997, London, UK.

Vorus, W.S., "A Flat Cylinder Theory for Vessel Impact and Steady Planing Resistance," Journal of Ship Research, Vol. 40, No. 2, 1996, pp. 89-106.

Wagner, H., "Über Stoß- und Gleitvorgänge an der Oberfläche von Flüssigkeiten," Zeitschrift für angewandte Mathematik und Mechanik, Vol. 12, No. 4, 1932, pp. 193-215.

Xu, G.D., Duan, W.Y., and Wu, G.X., "Numerical simulation of oblique water entry of an asymmetrical wedge," Ocean Engineering, Vol. 35. 2008, pp. 1597-1603.

Xu, G.D. and Wu, G.X., "Oblique water entry of a wedge with vortex shedding," Proceedings of the 30th International Workshop on Water Waves and Floating Bodies, 12-15 April, 2015, Bristol and Bath, UK.

Xu, L., Troesch, A.W. and Vorus, W.S., "Asymmetric Vessel Impact and Planing Hydrodynamics," Journal of Ship Research, Vol. 42, No. 3, 1998, pp. 187-198.

Yang, X.B. and Xu, G.D., "Numerical simulation of the oblique water entry of wedges with vortex shedding," Brodogradnja/Shipbuilding, Vol. 69, No. 4, 2018, pp. 69-83.

APPENDIX

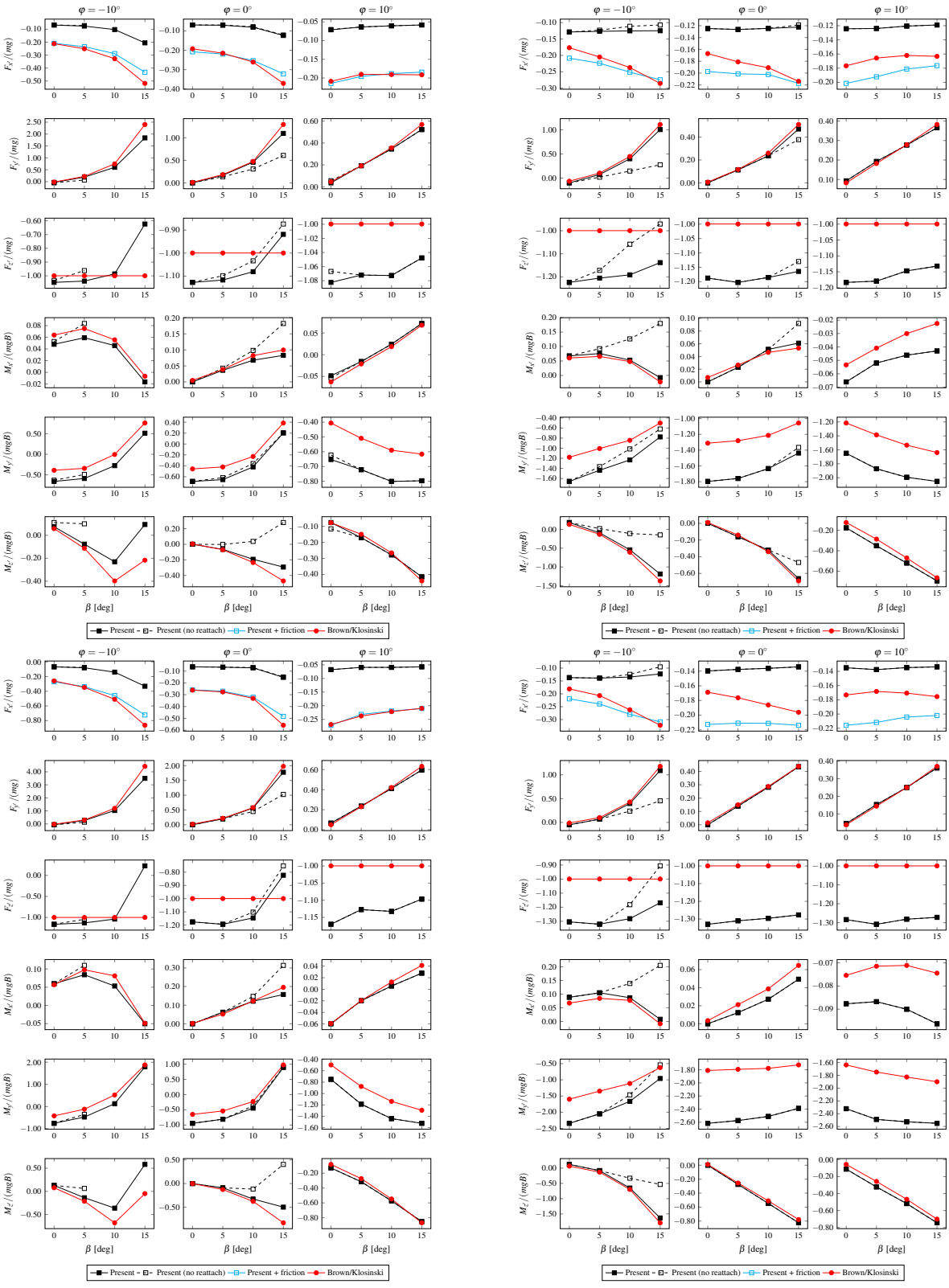

Figure 20: Full set of of calculated forces and moments for straight course drift simulations with $\theta = 3°$ (left) and $\theta = 6°$ (right) at $F_{nB} = 3.0$ (top) and $F_{nB} = 4.0$ (bottom) expressed in semi-body-fixed system and compared to experimental results.

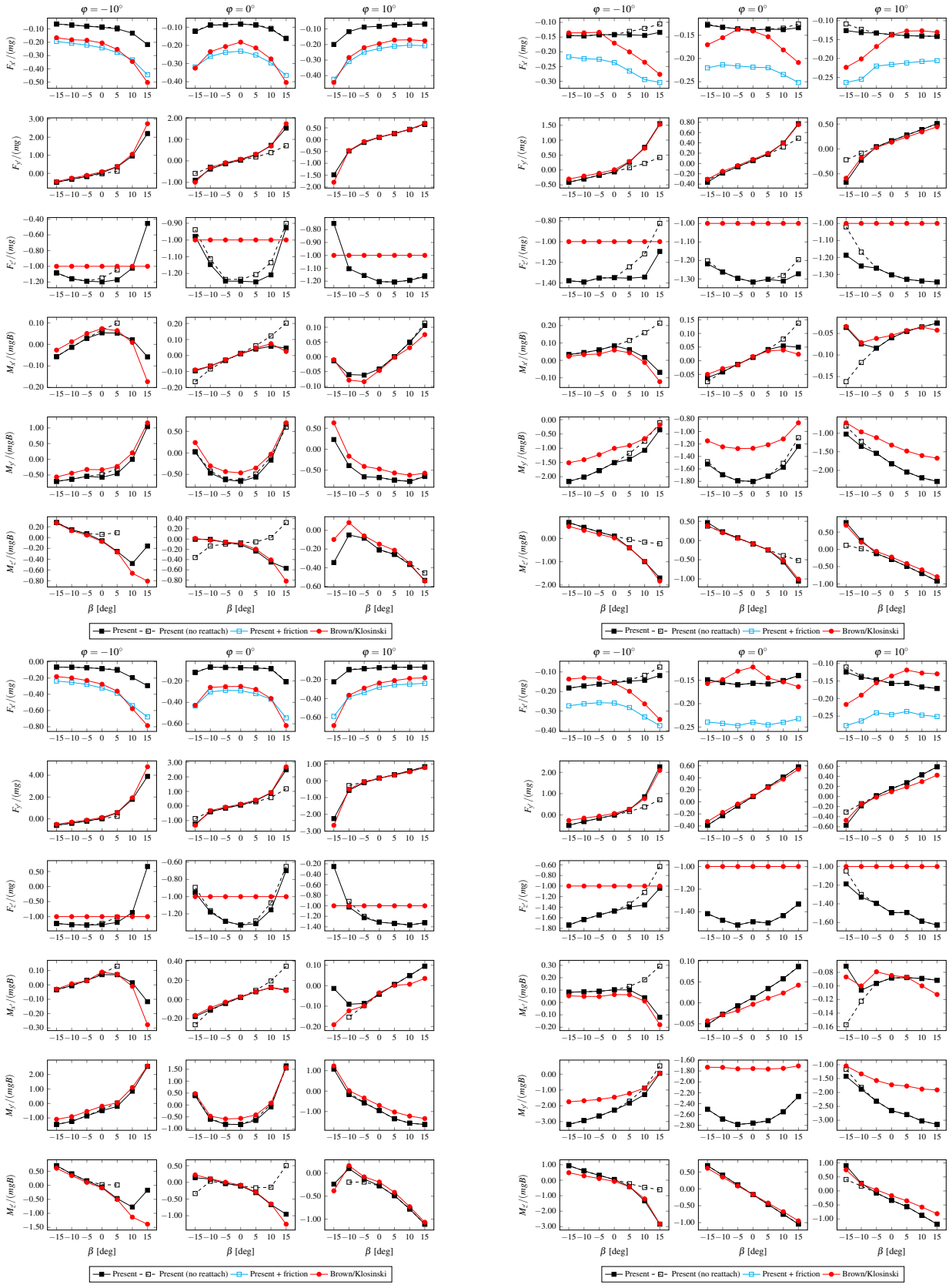

Figure 21: Full set of of calculated forces and moments for combined drift and yaw simulations with $\theta = 3°$ (left) and $\theta = 6°$ (right) at $F_{nB} = 3.0$ (top) and $F_{nB} = 4.0$ (bottom) expressed in semi-body-fixed system and compared to experimental results.

DISCUSSION

Andrés Cura Hochbaum, Technical University Berlin.

Many thanks to the authors for this very interesting paper, in which they describe their own 2D+t method and discuss the results in detail. Overall, they have succeeded in developing a practical and fast method for determining hydrodynamic forces and moments on a planing hull in steady drift and yaw motion. Some implemented tricks to mitigate drawbacks of the potential flow theory used, especially a "reattachment" technique, improved the method considerably and led to quite satisfactory results in situations of interest for manoeuvring prediction, at least for moderate drift angles. I would like to make the following comments.

1. As the authors note, the reason for the inaccurate prediction of the vertical force in general, and the side force and yaw moment at larger drift angles, is probably due to the fact that the potential flow does not capture separations along the keel. It does not seem easy to implement the mentioned vortex elements along the keel in a robust way, since it is only slightly oblique to the local flow. How should the length of the detachment region be chosen?

2. The method is not yet fully mature for predicting the running attitude of the planing boat and thus is used to calculate hydrodynamic forces at prescribed values of rise, trim, and heel. One could use it to calculate coefficients for manoeuvring prediction depending on drift angle and yaw rate for given floating conditions much faster than with a RANS code. For this purpose, however, appendages and the usual tunnels should be taken into account. Moreover, to calculate rudder angle dependent coefficients, the propeller effect must also be considered. Do you see the possibility of incorporating these effects?

3. I am surprised at how well the strip concept works for integrating the forces and moments on the hull, even though the ship is not that slender. Planing hulls often have even lower ratios than the Lpp/B = 5 of the present case. What do you expect in terms of accuracy for Lpp/B = 4 or smaller?

AUTHORS REPLY

Thank you very much for your comments and questions, each of which is addressed below:

1. The research on the topic mentioned in the paper (e.g. Semenov and Wu, 2018) is in the context of oblique water entry of wedges. It shows that a more realistic pressure distribution around the wedge apex can be obtained by enforcing a Kutta condition at the corner and modelling a vortex sheet, which is why we consider it as a potential improvement to the presented method. The concept is essentially equivalent to the common practice of modelling the wake of lifting surfaces in unsteady potential flow. In the case of the 2D BEM presented, it would mean that wake elements are shed from the keel over time and are frequently aligned with the local flow velocity within the sample plane. We agree that robustness issues may arise if the wake elements are too close to the hull surface, which is arguably more likely at small drift angles and small effective deadrise angles on the leeward side. However, the results of the present study suggest that these may also be the conditions in which the local negative pressure peak around the keel has the least effect on the final results. Therefore, further research is required to asses the conditions under which the use of such a technique is feasible and beneficial in the context of planing boat manoeuvring.

2. The method is specifically designed tp predict hydrodynamic forces on the hull. The current implementation allows the shape of the 2D hull boundary within the sample plane to be changed during a simulation. Thus, there is no restriction to prismatic hull shapes and propeller tunnels could generally be included in the flow solution. That being said, our focus to date has been on applications with jet propulsion and we have not yet tested or validated the method with such a hull geometry. The effects of appendages and the propulsion system cannot be considered directly in the flow solution. Instead, they need to be modelled separately and the resulting forces have to be added to the hull forces during manoeuvring simulations. An example of this approach in the case of jet propulsion can be found in the study by Algarín and Bula, (2021).

3. As can be seen from Table 4, a wide range of wetted length to beam ratios have been considered for the study reaching well below $L_w/B = 2$ in the cases with $F_{nB} = 4$ and $\theta = 6$. It is fair to say that the assumption of slenderness hardly applies to such low ratios. One reason why the results are still favourable can be seen in the artificial reduction of the sectional forces towards the stern (6), which partly accounts for 3D flow effects. Another possible reason is related to the mechanism of side force generation on a drifting planing hull, which can largely be seen as the difference between

the hydrodynamic lift on each side of the hull. Thus, if there are errors in the hydrodynamic lift prediction, but they are of similar magnitude on each side of the hull, they will cancel each other out. This explanation fits well with the general conclusion of the study that lateral forces are predicted more accurately than vertical forces. For a more detailed assessment of the influence of the slenderness assumption on the results, comparisons with a 3D flow solution would be required.